THE JOURNAL OF PHYSICAL CHEMISTRY C

ARTICLE

pubs.acs.org/JPCC

Chemically Modified Multiwalled Carbon Nanotubes Electrodes with Ferrocene Derivatives through Reactive Landing

Federico Pepi,*[,†] Alessandra Tata,[†] Stefania Garzoli,[†] Pierluigi Giacomello,[†] Rino Ragno,[†] Alexandros Patsilinakos,[†] Massimo Di Fusco,[†] Andrea D'Annibale,[‡] Salvatore Cannistraro,[§] Chiara Baldacchini,[§,⊥] Gabriele Favero,[†] Marco Frasconi,[†] and Franco Mazzei*[,†]

[†]Department of Chemistry and Drug Technologies and [‡]Department of Chemistry "Sapienza" University of Rome, P.le Aldo Moro 5, 00185 Rome, Italy

[§]Biophysics & Nanoscience Centre & CNISM Facoltà di Scienze, Università della Tuscia, I-01100 Viterbo, Italy

[⊥]CNR-IBAF, Via Marconi 2, 05010 Porano (TR), Italy

ABSTRACT:

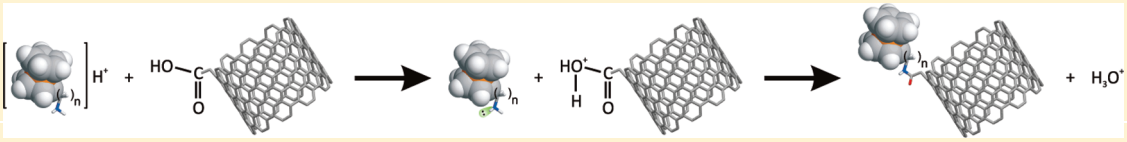

The immobilization of ferrocene's amino derivatives onto carboxyl-functionalized multiwalled carbon nanotubes (MWCNTs−COOH) electrodes has been carried out to test the ability of the ion reactive landing procedure to realize chemically modified electrodes. The ionic species involved in the ion reactive landing procedure were structurally and energetically characterized by the joint application of collisionally induced dissociation mass spectrometry and theoretical calculations. Furthermore, the modified surface was analyzed by spectroscopic and voltammetric techniques and the electron mediation of the ferrocene derivatives demonstrated in the presence of laccase. Data obtained put in evidence a strong interaction between the landed molecules and the MWCNTs surface.

INTRODUCTION

The performances of enzymatic electrodes can strongly benefit by enhancement of the electron transfer between redox center of the proteins and the electrode surface. To achieve this result two synergic strategies can be followed: i) the use of nanostructured materials (e.g., carbon nanotubes) to enhance the electrocatalytic properties of the electrodes, and ii) the chemical modification of the electrode surface by means of redox mediators to facilitate the communication with the redox center of the protein.[1−3]

Among the many surface modification procedures, ions soft landing could represent a viable alternative. Ion soft landing is defined as the deposition at low kinetic energies of specific molecular ions on a solid surface using a suitably modified mass spectrometer.[4−9] It has been demonstrated that the presence of functional groups on the surface allow the efficient covalent linking between the projectile molecule and the surface (reactive landing).[10−19] Despite the great interest aroused to this forefront surface modification technique, little is known about the ion-surface reaction mechanism.[20,21]

To test the potentiality of this technique to realize chemically modified electrodes and, at the same time, attempt to clarify the reactive landing mechanism, we taken into account the soft landing of ferrocene derivatives such as aminoferrocene (NH_2−Fc) and alkylaminoferrocenes (NH_2−$(CH_2)_n$Fc) (n = 3, 6, 11, 16) onto carboxyl-functionalized multiwalled carbon nanotubes (MWCNT−COOH) electrodes. Ferrocene derivatives have advantageous features such as stability in water solutions, sufficient vapor pressure and optimal electrochemical properties, which make them particularly suitable for mass spectrometric soft landing experiments as well as for the voltammetric analysis useful to check the electrochemical properties of the deposited redox molecule. Besides, because of the rapid heterogeneous electron transfer, the use of ferrocene-modified surfaces are attractive candidates for molecular electronics devices,[22] electrochemical pH sensor,[23] and biosensors.[24] In the last field, ferrocene-modified electrodes were widely employed as redox mediators between the electrode and the redox-active center of an enzyme.

The ionic species involved in the ion soft landing procedure were preliminarily structurally and energetically characterized by the joint application of collisionally induced dissociation mass spectrometry and theoretical calculations. Furthermore, the modified surface were analyzed by spectroscopic and voltammetric techniques.

To evaluate the feasibility of the soft landed modified electrodes to the development of electrochemical biosensors, laccase-modified electrodes have been realized. Moreover, the influence

Received: October 20, 2010
Revised: January 4, 2011
Published: February 24, 2011

of the chain length and interchain interactions on the electron transfer rate constant has been investigated.[25,26]

The data obtained by the electrochemical characterization of the aminoferrocene-modified electrodes clearly demonstrate a strong interaction between the landed molecules and the MWCNTs surfaces.

EXPERIMENTAL METHODS

All of the gases used were purchased from Matheson Gas Products Inc. with a stated purity of 99.9 mol %. Aminoferrocene, 1-ferrocenyl-3-aminopropane, 1-ferrocenyl-6-aminohexane, 1-ferrocenyl-11-aminoundecane, and 1-ferrocenyl-16-aminohexadecane were synthesized according to standard procedures.[27,28]

Mass Spectrometric Experiments. Triple quadrupole mass spectrometric CAD experiments were performed with a TSQ700 instrument from Thermo Finnigan Ltd. The ions were generated by positive electrospray ionization of 10^{-4} M ferrocene derivatives solutions in CH_3OH/H_2O (1:1) directly infused by a syringe pump at a flow of 20 μL/min. Typical operating conditions were: needle voltage 4.0 kV, flow rate 20 μL min^{-1}, capillary temperature 150 °C, capillary exit and skimmer voltage −80 and −120 V respectively, hexapole dc offset 1−2 V.

The ions generated in the source were driven into the collision cell, actually a RF-only hexapole, containing the neutral reagent. The collisionally activated dissociation (CAD) spectra were recorded using Ar as the target gas at pressures of about 0.1 mTorr and at collision energies ranging from 0 to 70 eV (laboratory frame). An upper limit of 2−3 eV for the kinetic energy of the reactant ion at nominal collision energy of 0 eV (laboratory frame) and an ion beam energy spread of about 1 eV can be estimated by using cutoff potentials. Laboratory ion energies (lab) are converted to center-of-mass (CM) energies by using the formula $E_{CM} = E_{LAB}\, m/(m + M)$, where m is the mass of neutral reactant and M is the mass of the ionic reagent. Experimental cross sections, σ_{tot}, were determined by the relation $I_R/I_{tot} = \exp^{(-\sigma nl)}$ where I_R is the intensities of the transmitted ion beam, I_{tot} is the total ion intensities, n is the number density of the neutral gas, and l is the effective gas cell length. Individual product cross sections, σ_p, were calculated by $\sigma_p = \sigma(I_p/I_{p_{tot}})$ where I_p represents the intensity of the product ion and $I_{p_{tot}}$ the total product ion intensities

The charged fragments and/or products were analyzed with the third quadrupole, scanned at a rate of 150 Th s^{-1}.

The soft landing experiments were performed with the same TSQ700 triple quadrupole mass spectrometer suitably modified as previously reported.[16,17]

The mean kinetic energy of the ion beam leaving the third quadrupole are measured by using cutoff potential and can be estimated as 10−12 eV. To estimate the ion beam width, different surfaces having a central round hole 0.5−3 mm in diameter were utilized. The ion beam intensity is practically unaffected by passing through the 2.5 mm hole.

ELECTROCHEMICAL MEASUREMENTS

The electrochemical experiments were performed with a MWCNT screen-printed electrode purchased from Dropsens (Oviedo, Spain). The MWCNTs electrodes are produced by thick-film hybrid technology on a ceramic substrate (L 33 × W 10 × H 0.5 mml; electric contacts, silver). The sensor consisted of an MWCNT surface (as working electrode, 4 mm diameter), an Ag/AgCl reference electrode (198 mV vs NHE) and a carbon counter electrode. The multiwalled carbon nanotube electrodes were carboxyl-functionalized with oxidizing acid (HNO_3 5 M for 2 h at 70 °C). The electrochemically determined microscopic area obtained from cyclic voltammograms of ferricyanide ion, the known diffusion coefficient, and the Randles−Sevcik equation was $A = (0.26 \pm 0.5)$ cm^2; all measurements of surface coverage were adjusted accordingly.

The electrodes were rinsed in phosphate buffer pH 7.0 (I = 0.1 M, with KCl) prior to voltammetric experiments. The electrochemical measurements were carried out in a thermostatted electrochemical cell with 0.01 M phosphate buffer pH 7.0 (I = 0.1 M, with KCl) under a nitrogen stream. The cyclic voltammograms were obtained by using the staircase method with current integration option using the Autolab electrochemical analyzer (from EcoChemie, Utrecht, The Netherlands).

The enzyme immobilization was performed by coating the functionalized electrodes with 5 μL of 1 mg mL^{-1} TvL solution in 0.1 M phosphate buffer pH 7.0 for 1 h. After washing, the electrodes were reacted with glutaric dialdehyde 10% (v/v) in 0.1 M phosphate buffer pH 7.0 for 3 h. The resulting electrodes were used for the experiments of biocatalytic reduction of oxygen in air saturated 0.1 M sodium citrated buffer solution pH 5.0.

Raman Spectroscopy Experiments. Raman spectra were recorded by using a Labram confocal micro-Raman system from Jobin−Yvon, equipped with a Peltier-cooled detector and a HeNe laser with an excitation wavelength of 633 nm. A spectrograph with a 1800 g mm^{-1} grating and a 50× objective allowing a resolution of about 5 cm^{-1} were used. The laser power was kept below 4 mW, to minimize sample damage.

Computational Methods. All calculations were performed using the general atomic and molecular electronic structure system (*GAMESS*) software[29] running on a 6 blades (8 Intel-Xeon E5520 2.27 GHz CPU and 24 GB DDR3 RAM each) cluster (48 CPU total) with a Debian GNU/Linux 5.03 operating system.

To calculate the geometries and energies of ferrocene and its derivatives, we used the B3LYP flavor of density functional theory (DFT), which includes the generalized gradient approximation and a component of the exact Hartree−Fock (HF) exchange.

The B3LYP method used predicts properties for ferrocene in reasonable agreement with available literature data.[30] The convergence criteria applied during the geometry optimizations were 10^{-4} Hartree/Bohr for the gradients.

The B3LYP/3-21G(d) low level of theory was first used to optimize the ferrocene geometries. Then 6-31G(d,p), 6-311G(d,p), and TZV(d,p) basis sets were used for the final geometry optimization starting from the 3-21G(d) optimized geometry.

The aminoferrocene derivatives were built starting by the optimized structures of ferrocene at B3LYP/TZV(d,p) level of theory. No restriction symmetries were used in all calculations.

The proton affinity of aminoferrocenes has been calculated at B3LYP/6-31G(d,p), B3LYP/6-311(d,p), and B3LYP/TZV(d,p) levels of theory.

Geometry optimizations and calculations of molecules as big as 1-ferrocenyl-11-aminoundecane were achieved using the 6-31G(d,p) basis set.

RESULTS AND DISCUSSION

Structural Characterization of $[NH_2{-}Fc]H^+$ and $[NH_2{-}(CH_2)_nFc]H^+$ Ions. *Theoretical Calculations.* To investigate the

Table 1. Relative Energies, Computed at the B3LYP/6-31G(d,p) Level of Theory Together with the Proton Affinity Value for Protonated Aminoferrocene and Alkylamino Ferrocenes

$[Fc-NH_2]H^+$	$Fc-NH_3^+$			$CpFeCpH^+NH_2$	$CpH^+FeCpNH_2$
total energy (Hartree)	−1706.05035			−1706.043405	−1706.042828
ΔE[tot] (Hartree)	−0.364745			−0.3578	−0.357224
ΔE[tot] (kcal/mol)	−228.880878			−224.52311	−224.161108
ZPE (kcal/mol)	126.304131			123.997466	123.363068
proton affinity (kcal/mol)	221.677981			219.626879	219.899275
$[Fc(CH_2)_3-NH_2]H^+$	$Fc(CH_2)_3NH_3^+$	$Fc(CH_2)_3NH_3^+$ "folded" a		$CpFeCpH^+NH_2$	$CpH^+FeCpNH_2$
total energy (Hartree)	−1823.917539	−1823.933078		−1823.892384	−1823.892563
ΔE[tot] (Hartree)	−0.373144	−0.388663		−0.347990	−0.348169
ΔE[tot] (kcal/mol)	−234.151415	−243.902444		−218.3668161	−218.4790921
ZPE (kcal/mol)	181.402233	181.046827		178.347027	178.669554
proton affinity (kcal/mol)	226.325253	236.431687		213.595859	213.385609
$[Fc(CH_2)_6-NH_2]H^+$	$Fc(CH_2)_6NH_3^+$	$Fc(CH_2)_6NH_3^+$ "folded"a	$Fc(CH_2)_6NH_3^+$ "folded"b	$CpFeCpH^+NH_2$	$CpH^+FeCpNH_2$
total energy (Hartree)	−1941.778785	−1941.793967	−1941.779677	−1941.756023	−1941.755393
ΔE[tot] (Hartree)	−0.372927	−0.388110	−0.373820	−0.351264	−0.349536
ΔE[tot] (kcal/mol)	−234.015379	−243.542542	−234.575331	−220.421762	−219.337151
ZPE (kcal/mol)	234.746299	235.239590	235.260813	232.367928	231.933963
proton affinity (kcal/mol)	226.229852	235.263725	226.275292	215.200048	214.363960
$[Fc(CH_2)_{11}-NH_2]H^+$	$Fc(CH_2)_{11}NH_3^+$	$Fc(CH_2)_{11}NH_3^+$ "folded"a	$Fc(CH_2)_{11}NH_3^+$ "folded"b	$CpFeCpH^+NH_2$	$CpH^+FeCpNH_2$
total energy (Hartree)	−2138.216137	−2138.230722	−2138.230028	−2138.192441	−2138.191734
ΔE[tot] (Hartree)	−0.373049	−0.3887633	−0.386939	−0.349895	−0.349187
ΔE[tot] (kcal/mol)	−234.091517	−243.243472	−242.807982	−219.562136	−219.118228
ZPE (kcal/mol)	324.808467	324.491575	324.329254	321.444360	321.533590
proton affinity (kcal/mol)	226.281069	235.749917	235.476738	214.369835	213.836696

structures of the $[NH_2-Fc]H^+$ and $[NH_2-(CH_2)_nFc]H^+$ (n = 3, 6, 11) ions, theoretical calculations were performed by using an approach based on the density functional theory using the hybrid B3LYP functional. The relative energies, computed at 0 K at the B3LYP/6-31G(d,p) level of theory are reported in Table 1 together with the proton affinity value for each isomeric species. The geometry optimization has been carried out with eclipsed, intermediate, and staggered structures. These conformations are almost isoenergetic with their energy differences never exceeding 0.4 kcal mol^{-1} and hence only the data relative to the more stable species were reported. The main optimized structures are shown in Figure 1. The amino-protonated isomer **I** is the most stable structure of protonated aminoferrocene even if the agostic form **II** and the species protonated on the amino-substituted cyclopentadienyl ring are less stable at least by about 2.0 kcal mol^{-1}.

The proton affinity of aminoferrocene protonated on the nitrogen atom is computed to be 221.7 kcal mol^{-1}.

In the case of 1-ferrocenyl-3-aminopropane the most stable structure **III**, protonated on the amino group, is characterized by a folded structure, named a, characterized by an intramolecular hydrogen bond between the NH_3 group and the cyclopentadienyl ring bearing the alkylamino substituent. This species is most stable than structure **IV**, were the linear chain moves away from the ferrocene moiety, by 10.1 kcal mol^{-1}.

The proton affinity of 1-ferrocenyl-3-aminopropane is computed to be 236.4 kcal mol^{-1}.

Proton affinities of 1-ferrocenyl-6-aminoexane and 1-ferrocenyl-11-aminoundecane are similar to that of 1-ferrocenyl-3-aminopropane. An additional isomer having a folded structure, named **b**, characterized by an hydrogen bond between protonated amino group and the unsubstituted cyclopentadienyl ring is also present in their energy potential surface. Protonated 1-ferrocenyl-6-aminoexane folded structure **VIb**, is less stable than isomer **Va** by 9.0 kcal mol^{-1} whereas the two isomeric species **VIIIa** and **IXb** of 1-ferrocenyl-11-aminoundecane are almost isoenergetic.

Mass Spectrometric Results. Protonated aminoferrocene, $[NH_2-Fc]H^+$ and alkylaminoferrocenes, $[NH_2-(CH_2)_nFc]H^+$ (n = 3, 6, 11, 16), were generated in the electrospray (ESI) source of a TSQ700 triple quadrupole mass spectrometer as reported in the Experimental Section. A representative ESI spectrum of 1-ferrocenyl-6-aminoexane is showed in Figure 2.

Low-energy collisionally activated dissociation (CAD) has been used to characterize the structure of the protonated ions. The relative intensities of the observed fragmentation at 6 eV center of mass collision energy are reported in Table 2.

Aminoferrocene CAD spectrum presents similar intensity of the fragments generated by the loss of NH_3, C_5H_6 and $NH_2C_5H_5$, thus indicating the formation of a mixed ionic population protonated on the amino group as well as on the cyclopentadienyl rings. This result is expected by considering the flat potential energy surface predicted by theoretical calculations.

The loss of NH_3 is progressively reduced in the CAD spectra of the alkylaminoferrocenes going from C3 to C16 being replaced by the loss of the alkylamine as the length of alkyl chain increases.

It is interesting to note that in these spectra the loss of the cyclopentadienyl ring bearing the alkylamino substituent is never

dx.doi.org/10.1021/jp1100472 |J. Phys. Chem. C 2011, 115, 4863–4871

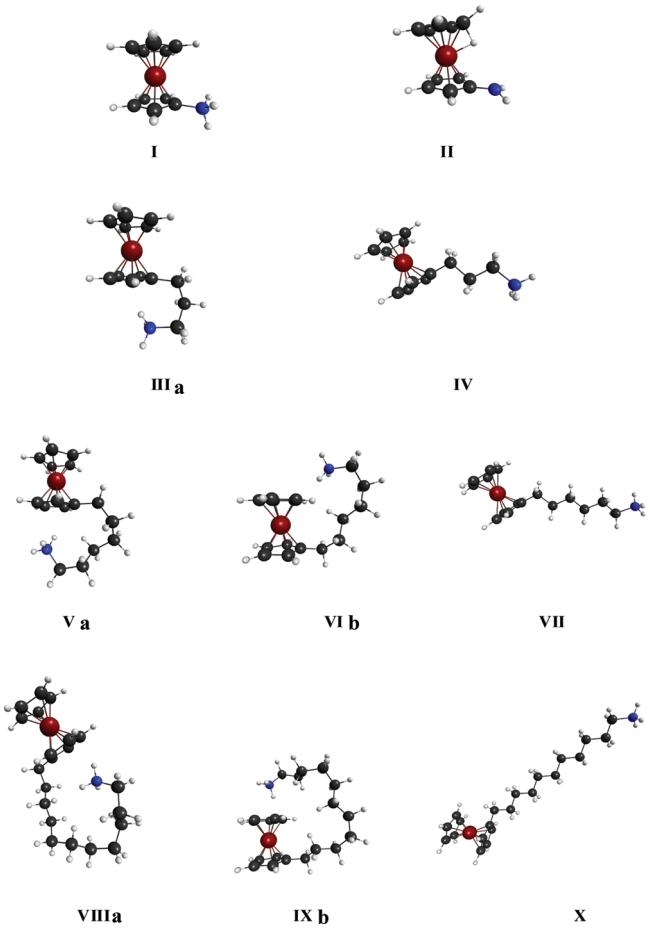

Figure 1. $[NH_2{-}Fc]H^+$ and $[NH_2{-}(CH_2)_nFc]H^+$ optimized structures.

observed whereas is always present the loss of unsubstituted cyclopentadiene ($-C_5H_6$).

The CAD spectrum of 1-ferrocenyl-3-aminopropane is dominated by the loss of C_5H_6. This fragmentation may arise from the folded structure **IIIa** throughout a proton transfer to the cyclopentadienyl group (Cp) assisted by the nitrogen lone pair that can easily coordinate the Fe^{2+} cation thus preserving the complex structure in the ionic fragment formed. In fact, by considering the proton affinity on the cyclopentadienyl rings, the loss of C_5H_6 can not be justified by the formation of the Cp protonated structures otherwise also the loss of amino-substituted cyclopentadiene has to be observed. Taking into account that the energy differences between linear and folded amino-protonated isomers is 10.1 kcal mol^{-1}, both these ionic species can be in principle present in the population of protonated 1-ferrocenyl-3-aminopropane.

The same construction can be applied to the ionic populations generated by protonation of 1-ferrocenyl-6-aminoexane, 1-ferrocenyl-11-aminoundecane and 1-ferrocenyl-16-aminoexadecane. In their CAD spectra, the relative intensity of the C_5H_6 loss decreases and correspondingly increases the alkylamino chain fragmentation. The decreased loss of cyclopentadiene can be ascribable to the competition with easier fragmentation channel as the alkyl chain is elongated but can also be justified by the existence of the folded structure **b**. In this isomeric form, the interaction between the alkylamino chain and the cyclopentadienyl ring can make less easy the loss of the latter species.

The relative dissociation energies of the fragmentation channels of protonated alkylaminoferrocenes generated in ESI condition were investigated by the energy resolved CAD spectra recorded at collision energies ranging from 0 to 9 eV (center of mass) reported in figure 3. The fragmentations leading to the loss of $CH_3(CH_2)_{n-2}NH_2$ (part a of Figure1) and $(CH_2)_n{-}NH_2$, (part c of Figure 1) are characterized by lower threshold energies on going from 1-ferrocenyl-3-aminopropane to 1-ferrocenyl-16-aminohexadecane as the alkyl chain is elongated.

The loss of the cyclopentadiene ring, (part b of Figure 1), is also influenced by the alkyl chain length even if 1-ferrocenyl-6-aminoexane shows a higher dissociation energies respect to 1-ferrocenyl-3-aminopropane probably due to the formation of the folded structure **b**. This dissociation represents the easiest fragmentation channel for all of the alkylaminoferrocenes investigated.

Reactive Landing Experiments. The whole unresolved isotopic pattern corresponding to protonated aminoferrocene derivatives was mass-selected with the first quadrupole and landed for different time periods ranging from 2 to 6 h, onto multiwalled carbon nanotubes electrodes activated by the oxidizing procedure. In a typical experiment a current of 100−300 pA was measured at the surface. The rough estimation of the ion current is due to the high noise registered by the picoammeter because of the shieldless surface introduction system. An additional acceleration potential was applied to the working MWCNTs electrode to guide the ions to the surface. To verify the influence of the acceleration potential on the deposition efficiency, several experiments were performed increasing the potential in the 0−100 V range. The electrochemical characterization of the modified surfaces (vide infra) evidenced an optimal deposition efficiency for all the ferrocene derivatives at −50 V, whereas lower amounts were found at −25 and −75 V. Furthermore, no deposition was observed at 0 V demonstrating that reactive landing of aminoferrocenes to the MWCNTs surface is promoted by the kinetic energy of the impinging ions. The following comparison experiments were conducted in order to asses the importance of the presence of a protonated amino group on the projectile ions and of the carboxyl functions on the target surface: i) reactive landing of protonated ferrocene generated in ESI condition onto activated MWCNTs electrodes, ii) reactive landing of aminoferrocene and alkylaminoferrocenes molecular ions, generated in N_2 chemical ionization condition, onto activated MWCNTs electrodes, and iii) reactive landing of protonated aminoferrocenes derivatives generated in ESI condition onto untreated MWCNTs electrodes. The different projectile ions were landed for different time periods ranging from 2 to 10 h and at different acceleration potential ranging from 0 to −100 V. The voltammetric analysis of the resulting electrodes evidenced that no linkage of the impinging ions to the nanotubes surfaces takes place in all these experimental conditions (vide infra).

Raman Spectroscopy Characterization of the Modified Electrodes. The effectiveness of the deposition method has been checked by means of Raman spectroscopy. Representative Raman spectra of 1-ferrocenyl-6-aminohexane soft-landed for 3 and 6 h onto MWCNTs electrodes are shown in Figure 4 (red and green curves, respectively). For comparison, the spectra of a bare MWCNT electrode (black curve) and of a drop of 1-ferrocenyl-6-aminohexane ethanol solution dried on glass (blue curve) are shown in the same figure.

These spectra are characterized by five sharp peaks located at 320, 400, 1060, 1105, and 3100 cm^{-1}, three broader peaks

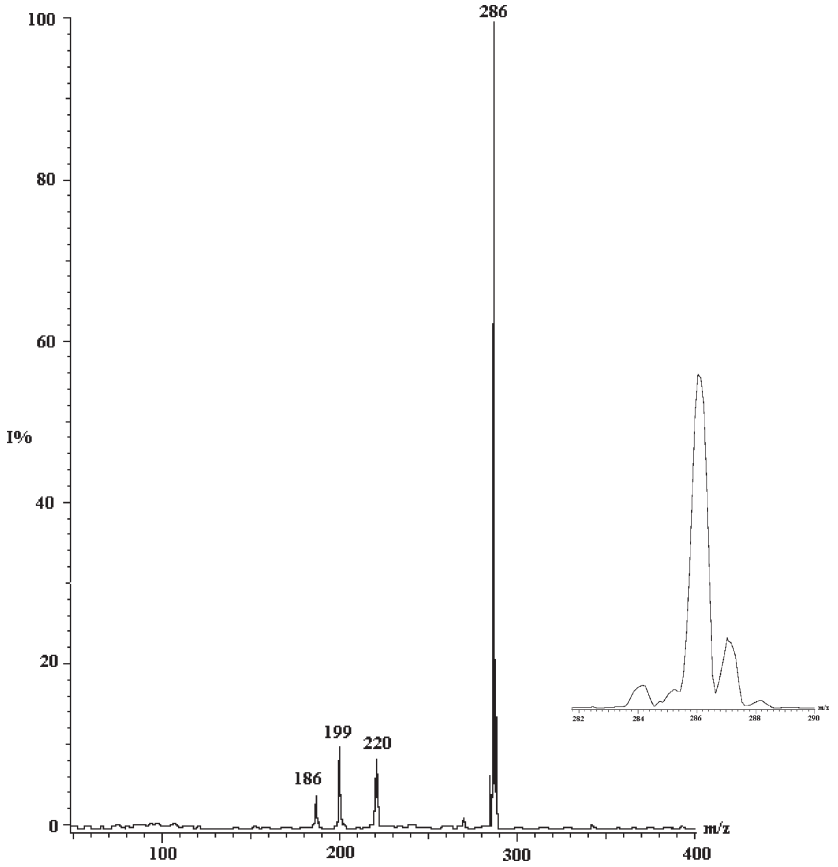

Figure 2. ESI mass spectrum of 1-ferrocenyl-6-aminohexane. Insert: magnification of the $[M-H]^+$ ion showing the Fe characteristic isotopes distribution.

Table 2. Low-Energy CAD of Protonated Aminoferrocene and Alkylaminoferrocenes

	fragment ions relative intensities (the neutral loss is indicated)					
parent ion	NH_3	C_5H_6	$NH_2C_5H_5$	C_5H_5Fe	$CH_3(CH_2)_{n\ -2}-NH_2$	$(CH_2)_n-NH_2$
$[Fc-NH_2]H^+$	24.6	25.4	27.9	22.1		
$[Fc(CH_2)_3-NH_2]H^+$	6.4	73.5			16.3	3.8
$[Fc(CH_2)_6-NH_2]H^+$	7.0	30.1			49.0	13.9
$[Fc(CH_2)_{11}-NH_2]H^+$	0.9	29.8			45.9	23.4
$[Fc(CH_2)_{16}-NH_2]H^+$		16.2			49.8	34.0

centered at around 1330, 1580, and 2660 cm^{-1}, and few minor signals. By comparing the spectra with that of a bare electrode, it clearly results that the broader peaks correspond to the graphene-like in-plane mode G band (1580 cm^{-1}), the defect-induced D band (1350 cm^{-1}) and its overtone G′ (2660 cm^{-1}), typical of carbon nanotubes.[31] The sharper peaks, whose intensity is shown to increase with the deposition time (red and green spectra in Figure 4), well match the main Raman features of 1-ferrocenyl-6-aminohexane (blue spectrum), currently attributed to the ferrocene ($Fe-C_{Cp}$; Cp, cyclopentadienyl) vibrational modes. In particular, the strong peaks at 1105 cm^{-1} (ring in-plane breathing mode) and at 320 cm^{-1} (Fe−C stretching) witness the presence of the cyclopentadienyl and of the metal atom, respectively.[32] The remaining signal at 1225 cm^{-1} do not correspond to any ferrocene or carbon nanotube modes and are common to both the landed and the dry 1-ferrocenyl-6-aminohexane Raman spectra. We suggest that they could be due to the alkyl chain linked to ferrocene (CH_2 scissoring and wagging vibrations at 1225 cm^{-1}[33]).

Electrochemical Characterization of the Ferrocene-Modified Electrodes. The evaluation of the redox properties of the ferrocene derivatives deposited onto the MWCNT's electrodes was performed by cyclic voltammetry. The voltammograms obtained by landing protonated aminoferrocenes ions are shown in part A of Figure 5. Voltammetric studies of the ferrocene-modified electrodes showed symmetric, well-defined reversible waves characteristic of the ferrocene/ferrocenium couple. The anodic-to-cathodic peak current ratio was close to unit, and a linear relationship between the scan rate and the current intensity was found, as expected for a surface-confined redox species.[34] The observed increase in the standard electrode potential (E^o) for ferrocene derivatives, is due to the oxidation process getting progressively more difficult with the length of their alkyl chain. As the oxidation process involves ion transfer to balance the charge

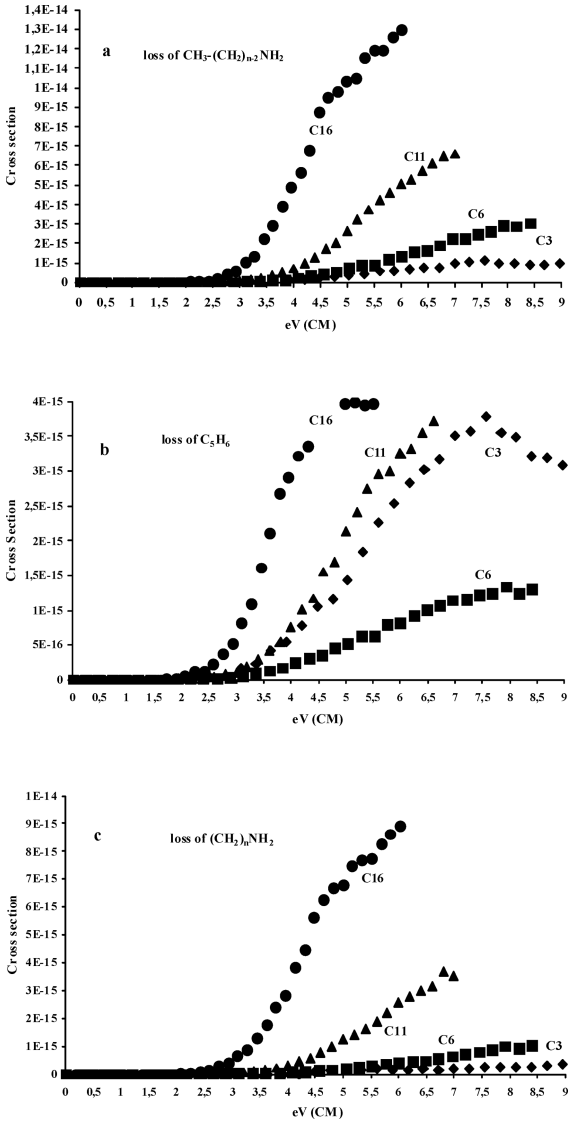

Figure 3. $[NH_2-(CH_2)_nFc]H^+$ (n = 3, 6, 11, 16) energy resolved CAD spectra recorded at center of mass (CM) collision energies ranging from 0 to 9 eV .

of the ferricinium ion it is possible that access of ions to the hydrophobic ferrocene is becoming more difficult with the alkyl length.[35]

Coulometric analysis of the redox wave indicates that the surface coverages (Γ) of the different alkylaminoferrocene molecules were between 0.33 ± 0.03 nmol cm^{-2} and 0.15 ± 0.02 nmol cm^{-2}.

The reported coverage is referred to the active electrochemical surface ($A = 0.26 \pm 0.5$ cm^2) obtained from the application of the Randles−Sevcik equation to cyclic voltammograms of ferricyanide ion carried in out in aqueous solution $(Fe(CN)_6)^{3-}$ 1.1 mM in KCl 0.1 M). In this environment, it is presumable that only a portion of the real surface is reachable because of the strong hydrophobicity of carbon nanotubes. In fact, by evaluating the electrochemically microscopic area in an organic solvent (such as acetonitrile) more prone than water to penetrate the inner space between one nanotube and one other, a significantly greater surface ($A = 1.28 \pm 0.07$ cm^2) can be measured.[36] So, when the MWCNT is modified by means of reactive landing it can be

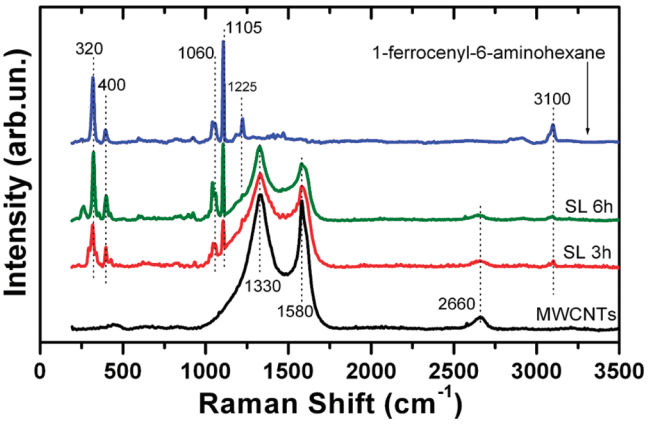

Figure 4. Raman spectra of: bare MWCNT electrode (black curve), 1-ferrocenyl-6-aminohexane after 3 and 6 h deposition time (red and green curves, respectively), drop of 1-ferrocenyl-6-aminohexane solution in ethanol dry on glass (blue curve).

hypothesized that the surface exposed to the interaction with the ion beam should be greater with respect to that one calculated in aqueous solution thus resulting in an apparent surface coverage clearly overestimated. Moreover, by using the same deposition conditions (i.e., ion current, time deposition, and acceleration potential) the average apparent surface coverage (for at least six reactive landing experiments) measured for the different ferrocene derivatives can be compared (part B of Figure 5). It is interesting to note that the surface coverage depends on the number of methylene groups in the aminoferrocenes alkyl chain.

The maximum surface coverage is measured for 1-ferrocenyl-6-aminohexane, whereas the amount of deposition is strongly decreased in 1-ferrocenyl-11-aminoundecane and 1-ferrocenyl-16-amino hexadecane. This behavior seems to be strictly connected with the dissociation threshold energies derived by the energy resolved CAD spectra. 1-ferrocenil-6-aminohexane is characterized by higher dissociation energy than the other derivatives and hence, by using the same acceleration potential, its reactive landing process is less affected by concomitant dissociation processes.

The lower amount of aminoferrocene deposition may be due to the delocalization of the nitrogen lone pair to the cyclopentadienyl π system or to a minor extent of the protonation on the amino group.

In addition, any attempts to reactive landing protonated ferrocene and alkylaminoferrocenes molecular ions failed, as well as the experiments carried out by landing protonated aminoferrocenes ions onto untreated MWCNTs electrodes. In all of these experiments, the cyclic voltammetric analysis of the modified MWCNTs surfaces evidenced only a low voltammetric current during the first scan, which quickly disappears. This clearly demonstrates that the ions can be deposited onto the electrode surface but no covalent linkage by reactive landing takes place in the absence of a protonated amino group on the ferrocene moiety and of nanotubes COOH functional groups.

It is worth noting that aminoferrocene reactive landing leads to the formation of a strongly bound layer that maintains its redox activity for several days even after several consecutive voltammetric experiments in aqueous buffer solution.

The strong interaction between soft-landed aminoferroecene derivatives and MWCNTs electrodes is also proved by the

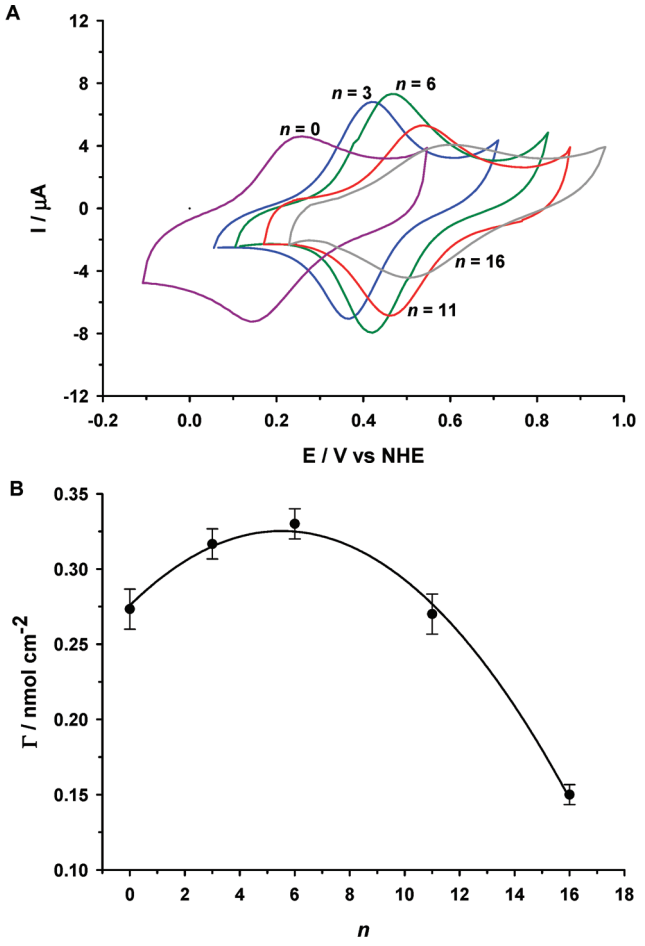

Figure 5. (A) Cyclic voltammograms of differently modified MWCNT electrodes by reactive landing of protonated: aminoferrocene (purple), 1-ferrocenil-3-aminopropane (blue), 1-ferrocenil-6-aminohexane (green),1-ferrocenil-11-aminoundecane (red), and 1-ferrocenil-16-aminohexadecane (gray) generated in ESI condition. Data were recorded in 0.01 M phosphate buffer pH 7.0 (I = 0.1 with KCl), under N_2 at 25 °C, with a potential scan rate of 100 mV s^{-1}. (B) Dependence of surface coverage of landed ferrocene derivatives as a function of the alkyl chain length.

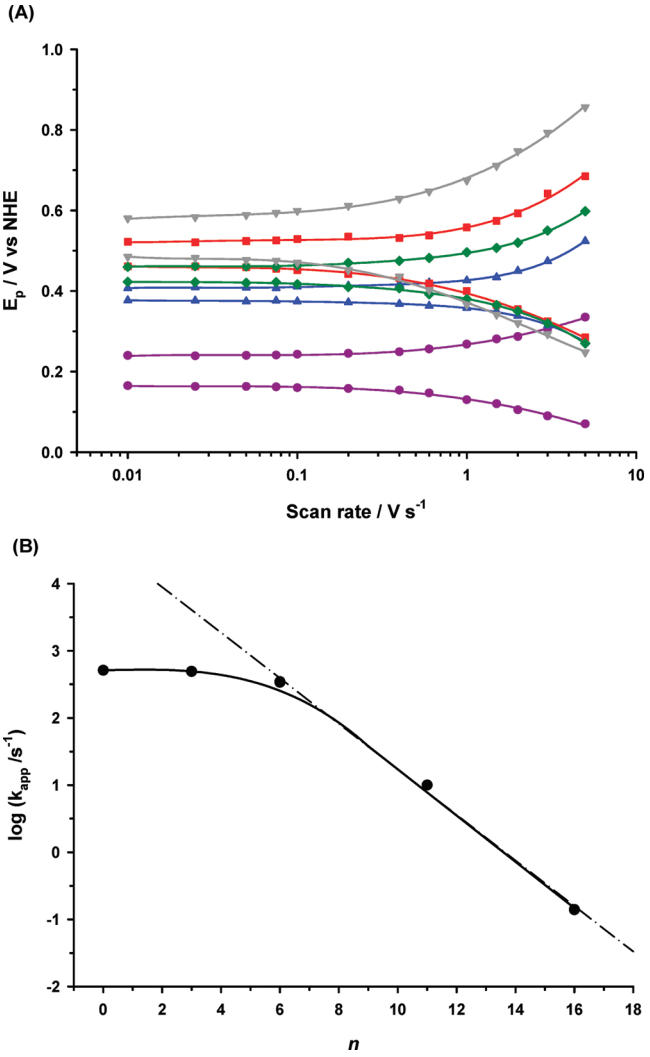

Figure 6. (A) Trumpet plots for the differently modified MWCNTs electrodes by reactive landing of: aminoferrocene (purple), 1-ferrocenil-3-aminopropane (blue), 1-ferrocenil-6-aminohexane (green),1-ferrocenil-11-aminoundecane (red), and 1-ferrocenil-16-aminohexadecane (gray). Cathodic and anodic peak potentials were determined from voltammograms that were recorded in 0.01 M phosphate buffer pH 7.0 (I = 0.1 with KCl), under N_2 at 25 °C. (B) Logarithmic plot of the observed ET rate constants ($\Delta G^0 = 0$) of soft landed ferrocene derivatives as a function of the number of methylene groups in the alkyl chain ($H_2N(CH_2)_nFC$).

stability of the surface coverage value versus rinsing procedures as reported in the Experimental Section.

Furthermore, from the shift of the anodic and cathodic peak position as a function of the scan rate, the electron transfer rate constants (k_{app}) were evaluated for the different aminoferrocene alkyl chains. These data were fitted using a Butler−Volmer equation for a surface confined redox reaction,[37] and the result of the fit is reported in Figure 6. The increase of the chain length has a dramatic effect upon the rate constant causing a reduction of the constant for each methylene group in the alkyl chain. The electron transfer kinetic of the ferrocene derivatives is strongly influenced by the distance between the redox center and the electrode surface.

Laccase-Based Biosensor. In view of the application of ferrocene-modified MWCNTs electrodes as a component of an electrochemical biosensor, we have chosen laccase to examine the mediated electron transfer for the oxygen reduction. As a well studied multicopper oxidase, we have selected laccase from *Trametes versicolor* that presents an accessible active site for redox mediators, and laccase is a good candidate for investigating its mediated electron transfer at the ferrocene-modified surface.

Figure 7 depicts the cyclic voltammograms corresponding to the biocatalyzed reduction of oxygen by the laccase immobilized (using the glutaraldehyde coupling) on different functionalized alkylamino ferrocene-modified MWCNTs electrodes. The behavior is typical of a catalytic process due to the electron mediation of the ferrocene anchored to the surface by the alkyl chain in the presence of the enzyme.[38] Furthermore, a maximum catalytic cathodic current was achieved for the ferrocene alkyl chains with 6 and 11 methylene groups, corresponding to a higher mobility of the ferrocene moiety and to the appropriate alkyl chain length capable to interact with the reactive center of the enzyme.

Reactive Landing Mechanism. The formation of a strong interaction between the aminoferrocene derivatives and the functionalized nanotubes only in the presence of a protonated amino group on the projectile ions and of a COOH function on

dx.doi.org/10.1021/jp1100472 |J. Phys. Chem. C 2011, 115, 4863–4871

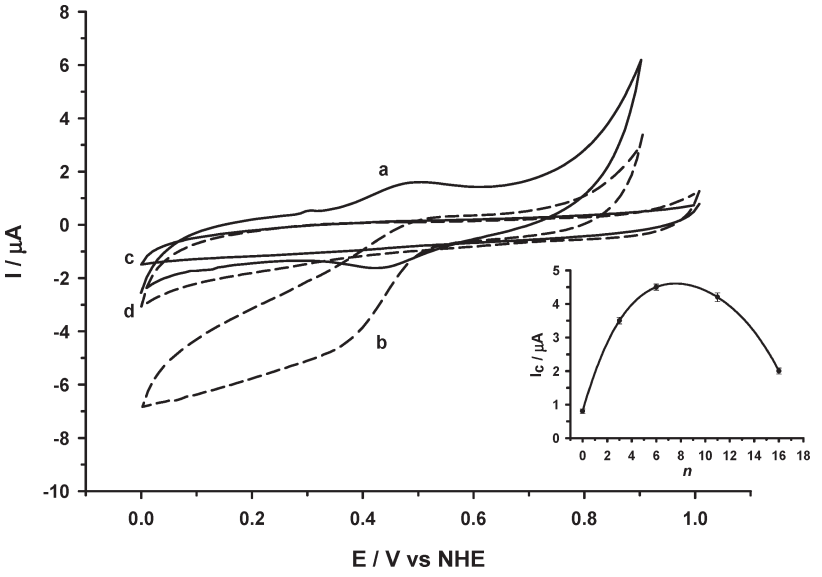

Figure 7. Cyclic voltammograms of laccase from *Trametes versicolor* with (a, b) and without electrode surface modification by reactive landing of 1-ferrocenil-6-amino hexane (c, d), under N_2 (solid line) and air saturated (dashed line) 0.1 M sodium citrated buffer solution pH 5.0. Data were recorded at 25 °C with a potential scan rate of 10 mV s^{-1}. Insert: behavior of the catalytic current for the O_2 reduction as a function of the of the number of methylene groups in the alkyl chain $(H_2N(CH_2)_nFC)$.

the surface may be justified by the formation of a covalent amide bond or by an ionic interaction between the NH_3^+ moiety and the COO^- anion eventually present in the nanotubes surface. Nevertheless, the strength of the deposited aminoferrocenes layer versus the rinsing procedures as well as the time stability of the modified electrodes voltammetric signals seem to exclude the formation of an ionic interaction that should be easily broken in the ionic aqueous medium used. On the contrary, some indirect evidence seem to support the formation of a covalent bond and the following acid-catalyzed reactive landing mechanism may be hypothesized taking into account the results of previous studies on comparable systems.[19]

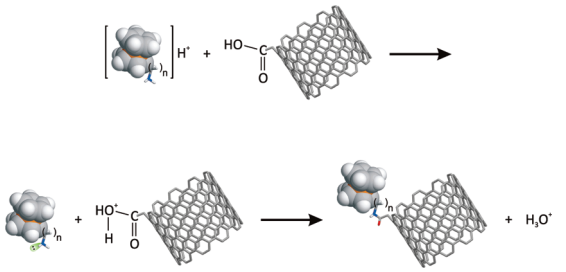

The first step of the reaction is the endothermic proton transfer from the more basic amino group of the projectile ion to the carboxylic function onto the nanotubes surface. By considering that the proton affinity of acetic acid is 187.3 kcal mol^{-1}, this reaction is endothermic by at least 39.0 and 49.1 kcal mol^{-1} in the case of protonated aminoferrocene and alkylamino ferrocenes derivatives, respectively. The existence of this energy barrier justifies the necessity of an additional acceleration potential to the projectile ion produced by the soft electrospray ionization technique.

The protonated COOH moiety is now activated to undergo the nucleophilic attack by the nitrogen lone pair and the amide bond can be formed by losing the additional proton to the exit water molecule or to other adventitious species present onto the surfaces. In this context, the lower amount of aminoferrocene than 1-ferrocenyl-3-aminopropane and 1-ferrocenyl-6-amino-hexane can be justified by its lower nucleophilicity due to the delocalization of the nitrogen lone pair to the cyclopentadienyl π system.

CONCLUSIONS

Multiwalled carbon nanotubes electrodes were functionalized with electroactive molecules by using the mass spectrometric reactive landing procedure with the aim to develop improved electrochemical transducers with potential applications in biosensors and biofuel cells. Structurally well characterized aminoferrocene and alkylaminoferrocenes protonated cations were successfully landed onto the carbon nanotubes surfaces as demonstrated by spectroscopic and voltammetric techniques. The electron mediation of the ferrocene derivatives strongly anchored to the electrode surface was observed in the presence of laccase. The whole picture emerging from the experimental results allow the mechanism of the ion−solid reaction to be hypothesized.

AUTHOR INFORMATION

Corresponding Author

*(F.P.) Phone: +390649913119. Fax: +390649913602. E-mail: Federico.Pepi@uniroma1.it. (F.M.) Phone: +3906499-13225. Fax: +390649913133. E-mail: Franco.Mazzei@uniroma1.it.

ACKNOWLEDGMENT

Work carried out with the financial support of "Sapienza" University of Rome and of the European Commission under contract number 017350.

REFERENCES

(1) Armstrong, F. A.; Wilson, G. S. *Electrochim. Acta* **2000**, *45*, 2623–2645.
(2) Katz, E.; Willner, I. *Angew. Chem., Int. Ed.* **2004**, *43*, 6042–6108.
(3) Wang, J. *Chem. Rev.* **2008**, *108*, 814–825.
(4) Miller, S. A.; Luo, H.; Jiang, X.; Rohrs, H. W.; Cooks, R. G. *Int. J. Mass Spectrom. Ion Processes* **1997**, *160*, 83–105.
(5) Pradeep, T.; Feng, B.; Ast, T.; Patrick, J. S.; Cooks, R. G.; Pachuta, S. J. *J. Am. Soc. Mass. Spectrom.* **1995**, *6*, 187–194.
(6) Shen, J. W.; Grill, V.; Evans, C.; Cooks, R. G. *J. Mass Spectrom.* **1999**, *34*, 354–363.
(7) Wade, N.; Pradeep, T.; Shen, J. W.; Cooks, R. G. *Rapid Commun. Mass Spectrom.* **1999**, *13*, 986–993.
(8) Rauschenbach, S.; Vogelgesang, R.; Malinowsky, N.; Gerlach, J. W.; Benyoucef, M.; Costantini, G.; Deng, Z.; Thontasen, N.; Kern, K. *ACS Nano* **2009**, *3*, 2901–2910.
(9) Thontasen, N.; Levita, G.; Malinowsky, N.; Deng, Z.; Rauschenbach, S.; Kern, K. *J. Phys. Chem. C* **2010**, *114*, 17768–17772.
(10) Gu, C.; Wysocki, V. H.; Harada, A.; Takaya, H.; Kumadaki, I. *J. Am. Chem. Soc.* **1999**, *121*, 10554–10562.
(11) Wade, N.; Gologan, B.; Vincze, A.; Cooks, R. G.; Sullivan, D. M.; Bruening, M. L. *Langmuir* **2002**, *18*, 4799–4808.
(12) Evans, C.; Wade, N.; Pepi, F.; Strossman, G.; Schuerlein, T.; Cooks, R. G.. *Anal. Chem.* **2002**, *74*, 317–323.
(13) Wang, P.; Hadjar, O.; Laskin, J. *J. Am. Chem. Soc.* **2007**, *129*, 8682–8683.
(14) Wang, P.; Hadjar, O.; Gassman, P. L.; Laskin, J. *Phys. Chem. Chem. Phys.* **2008**, *10*, 1079–1090.
(15) Wang, P.; Laskin, J. *Angew. Chem., Int. Ed.* **2008**, *47*, 6678–6680.
(16) Mazzei, F.; Favero, G.; Frasconi, M.; Tata, A.; Pepi, F. *Chem.—Eur. J.* **2009**, *15*, 7359–7367.
(17) Mazzei, F.; Pepi, F.; Frasconi, M.; Tata, A.; Ricci, A.; Delle Noci, S.; Favero, G. *Chem. Commun.* **2007**, 3494–3496.
(18) Mazzei, F.; Pepi, F.; Frasconi, M.; Tata, A.; Favero, G.; Tuccitto, N.; Licciardello, A. *Anal. Chem.* **2008**, *80*, 5937–5944.
(19) Hu, Q.; Wang, P.; Gassman, P. L.; Laskin, J. *Anal. Chem.* **2009**, *81*, 7302–7308.
(20) Volny, M.; Elam, W. T.; Branca, A.; Ratner, B. D.; Turecek, F. *Anal. Chem.* **2005**, *77*, 4890–4896.
(21) Blacken, G. R.; Volný, M.; Vaisar, T.; Sadílek, M.; Turecek, F. *Anal. Chem.* **2007**, *79*, 5449–5456.
(22) Yu, J.; Shapter, J. G.; Johnston, M. R.; Quinton, J. S.; Gooding, J. *J. Electrochim. Acta* **2007**, *52*, 6206–6218.
(23) Hickman, J. J.; Ofer, D.; Laibinis, P. E.; Whitesides, G. M.; Wrighton, M. S. *Science* **1991**, *252*, 688–691.
(24) Willner, I.; Katz, E. *Angew. Chem., Int. Ed.* **2000**, *39*, 1180–1218.
(25) Lee, L. Y. S.; Sutherland, T. C.; Rucareanu, S.; Lennox, R. B. *Langmuir* **2006**, *22*, 4438–4444.
(26) Napper, A. M.; Liu, H.; Waldeck, D. H. *J. Phys. Chem. B* **2001**, *105*, 7699–7707.
(27) Métay, E.; Duclos, M. C.; Pellet-Rostaing, S.; Lemaire, M.; Schulz, J.; Kannappan, R.; Bucher, C.; Saint-Aman, E.; Chaix, C. *Eur. J. Org. Chem.* **2008**, 4304–4312.
(28) Scriven, E. F. V.; Turnbull, K. *Chem. Rev.* **1988**, *88*, 297–368.
(29) Schmidt, M. W.; Baldridge, K. K.; Boatz, J. A.; Elbert, S. T.; Gordon, M. S.; Jensen., J. H.; Koseki, S.; Matsunaga, N.; Nguyen, K. A.; Su, S.; Windus, T. L.; Dupuis, M.; Montgomery, J. A. *J. Comput. Chem.* **1993**, *14*, 1347–1363.
(30) Xu, Z.-F.; Xie, Y.; Feng, W.-L.; Schaefer, H. F., III *J. Phys. Chem. A* **2003**, *107*, 2716–2729.
(31) Dresselhaus, M. S.; Dresselhaus, G.; Jorio, A.; Souza Filho, A. G.; Saito, R. *Carbon* **2002**, *40*, 2043–2061.
(32) Shimei, J.; Yue, W. *Spectrochim. Acta, Part A* **1999**, *55*, 1025–1033.
(33) Rabolt, J. F.; Hofer, D.; Miller, R. D.; Fickes, G. N. *Macromolecules* **1986**, *19*, 611–616.
(34) Savéant, J. M. *Elements of Molecular and Biomolecular Electrochemistry*; Hoboken: Wiley Interscience, 2006.
(35) Liu, J.; Paddon-Row, M. N.; Gooding, J. J. *J. Phys. Chem. B* **2004**, *108*, 8460–8466.
(36) Yu, J.; Shapter, J. G.; Johnston, M. R.; Quinton, J. S.; Gooding, J. J. *Electrochim. Acta* **2007**, *52*, 6206–6211.
(37) Laviron, E. J. *Electroanal. Chem.* **1979**, *101*, 19–28.
(38) Frasconi, M.; Boer, H.; Koivula, A.; Mazzei, F. *Electrochim. Acta* **2010**, *56*, 817–827.